OPEN ACCESS

DESIGN AND DISTRIBUTED CONTROL OF ELECTROMECHANICAL SYSTEMS FOR MULTIROTOR UAV SWARMS FOR LOW-ALTITUDE COOPERATIVE COMMUNICATION

Dongqin Zhou [0009-0008-6032-9314]
Chongqing Vocational and Technical University of Mechatronics, Chongqing 400000, China

Abstract - The paper addresses the critical gap between electromechanical platform constraints and dynamic communication demands in low-altitude multi-rotor UAV swarms, where conventional control theories often ignore physical layer coupling such as energy, thermal, and electromagnetic compatibility. To tackle this, a multidisciplinary collaborative optimization framework is constructed, transforming top-level relay tasks into tangible design parameters including rotor diameter and battery density. Subsequently, a distributed robust consensus algorithm integrated with a relative-threshold event-triggered mechanism is proposed to alleviate bandwidth scarcity. Compared to standard Leader-Follower and ideal Consensus baselines under identical wind disturbance and packet loss conditions, the presented framework reduces the formation root mean square error by over 60% and communication bandwidth consumption by more than 99%, while simultaneously improving network connectivity and task completion rates.

Keywords: UAV swarm, Low-altitude cooperative communication, Distributed control, Multidisciplinary optimization design, Cross-domain resource scheduling.

1. Introduction

With the rapid development of unmanned systems, drones, as a kind of intelligent unmanned platform, have become intelligent carriers of various emerging technologies. Multi-rotor drones have a wide range of application prospects in many fields such as logistics distribution, emergency rescue, and environmental monitoring, because they can take off and land vertically [1]. They also have advantages such as flexible operation, but single drones have limitations in application. These include limitations in endurance, payload capacity, and mission range, making it impossible to complete tasks in low-altitude operations with low complexity. Therefore, in this context, multi-rotor drones can achieve the overall performance of the drone system through core features such as multi-drone collaboration, information sharing, and task allocation. They have obvious advantages compared to single drones.

On the other hand, low-altitude airspace has become an important component of current communication networks. Resource scarcity and intense spectrum competition are among the challenges of low-altitude airspace, especially in complex environments such as disaster areas, mountainous regions, and canyons, where ground communications are extremely vulnerable to obstruction and damage. Therefore, maintaining a stable low-altitude communication network is even more difficult. The development of UAV technology is closely related to low-altitude communication technology. Therefore, this paper focuses on these two characteristics, integrating multi-rotor UAV swarms and electromechanical system design.

Our research on the dynamic and uncertain tasks of low-altitude communication aims to enable UAV swarms to maintain coordination, thereby promoting the development of multi-agent systems. In response to the problems in low-altitude communication, we have carried out efficient integration and design of UAV platforms. In addition, we also consider improving the consistency of distributed systems, thereby improving the scalability and robustness of the overall low-altitude logistics tasks [2].

The distinct contributions over existing works are threefold: (i) a closed-loop co-design that embeds electromechanical physics into swarm decision-making, which is absent in Refs. [16-18]; (ii) an adaptive triggering rule where the threshold is dynamically proportional to the consensus error,

dx.doi.org/10.17683/ijomam/issue25/v2.9

reducing redundant transmissions; and (iii) a potential-game-based scheduler that guarantees Nash equilibrium.

How to jointly optimize the electromechanical platform parameters, distributed flight control laws, and communication resource allocation to maximize mission effectiveness under severe low-altitude constraints? To address this within a consistent framework, a three-layer hierarchical workflow is established. The first layer transforms top-level communication tasks into quantifiable physical design variables (e.g., rotor diameter, battery density). The second layer embeds these physical constraints into a robust consensus controller with an event-triggered mechanism. The third layer formulates a game-theoretic scheduler that adjusts bandwidth and computing power based on the real-time energy states derived from the first layer. This cascaded structure ensures that each module's output serves as a hard constraint for the subsequent module, rather than operating as independent parallel topics.

2. Literature Review

2.1 Development of Unmanned Aerial Vehicle (UAV) Swarms

The earliest drone swarm technology was to simulate the cooperative behavior of birds, fish and other natural creatures. The U.S. Defense Advanced Research Projects Agency (DARPA) first proposed the concept of the Elf Project and the Loyal Wingman. It first applied drone swarm technology to distributed combat behavior in the military field. In the civilian field, drone swarms have also been used for light shows. Currently in China, it is possible to achieve the coordinated flight of more than 1,000 drone swarms. The existing drone swarm control architectures are mainly centralized, distributed and decentralized. The centralized architecture mainly relies on a central node to achieve global control optimization. However, these nodes will have a certain risk of single point failure and communication bottleneck. The decentralized architecture will compromise through different levels of structure [3]. The distributed architecture is in the absence of a central node, where each node unit will make decisions based on its own local information. This is also the current research direction. Most of the current research is to conduct distributed drone swarm exercises and control under ideal communication environments and fixed dynamic models. However, there is no analysis and exploration of the complex communication environment at low altitudes and the actual drone relay system.

2.2. Development of Low-Altitude Cooperative Communication Networks

Low-altitude cooperative communication network is a mobile self-organizing network. The difficulty of this network lies in how to manage the network topology and how to design the routing communication protocol, so as to realize the allocation of resources and communication and optimization at different levels [4]. For example, in the problem of the deployment location of UAV nodes, airborne base stations or relays are often used as deployment locations to achieve maximum network content coverage [5]. However, the current research status is that most UAV nodes are regarded as an ideal, controllable communication terminal, ignoring the physical attributes of the UAV platform itself, including electromechanical characteristics, energy constraints, flight control and the coupling relationship between communication tasks [6]. In actual operation, the maneuverability, payload capacity and endurance of UAVs are the core determining factors for their flexibility and service durability as communication nodes. Communication tasks generate power consumption and heat, and have certain requirements for electromagnetic compatibility. This characteristic also affects the flight status of UAVs and the overall design framework of their electromechanical systems [7]. Therefore, it is currently being considered to perform relative positioning and mutual sensing of signals between UAVs, so as to reduce the dependence on additional sensors. In the process of distributed control, the quality of the communication link can be modelled explicitly, thereby realizing the joint optimization of communication control and flight control [8, 9].

2.3 Current Research Challenges

Currently, there are still significant challenges in achieving high-efficiency communication in UAV swarms. First, a reasonable collaborative optimization design of the UAV electromechanical system is required. This design needs to consider how to design performance indicators that meet the current single-unit and swarm-related requirements under the existing low-altitude collaborative communication task environment, such as endurance, payload, and communication load, electromagnetic compatibility, and other indicators [10, 11]. This should be implemented according to the environment. Multi-dimensional integrated subsystem collaborative optimization is also needed. On the other hand, it is also necessary to consider how to carry out distributed collaborative control under the condition of many coupling constraints [12-14].

In such a modeling environment, there are often high uncertainties and external interferences, and the actuators often face dynamic constraints. In addition, the time delay and intermittent communication problems caused by low-altitude communication need to be considered. We need to consider how to design a distributed swarm control method that conforms to the distributed control rules under the constraint of limited bandwidth [15].

Therefore, in this context, researchers Liu et al. [16] constructed the iSAC architecture by treating communication and sensing as a joint optimization problem. This architecture can use the same set of radio frequency front-ends to perform two tasks, including target detection and information transmission. Ding et al. [17] combined UAV relay optimization algorithms in their research. Based on this, they optimized the reflection phase and other parameters. The algorithm was adjusted to improve spectral efficiency and expand the communication range. Alam et al. [18] considered the complex electromagnetic environment in their research and proposed a communication scheme that can be modeled based on such electromagnetic interference. They optimized the joint beamforming and flight trajectory information to improve spectral efficiency and signal stability.

While previous studies, such as the iSAC architecture by Liu et al. [16] and the relay optimization by Ding et al. [17], effectively treat communication and sensing or phase shifts, they universally model UAVs as ideal terminals without considering the electromechanical feedback (e.g., extra communication payload increasing power consumption and altering flight dynamics). In contrast, the proposed framework explicitly models these physical couplings and integrates them into the distributed control loop, thereby providing a more realistic and practical solution for low-altitude scenarios where energy and thermal states are tightly bounded to communication tasks.

3. Electromechanical System Design and Distributed Control System for Multi-rotor UAV Swarms

3.1 Model Framework

We represent the low-altitude communication task as a multi-dimensional set of constraints. Specifically, it can be represented as T = {A, Q, D, R} , where A represents the area covered by the target in three-dimensional space, which is described by a set of polyhedra , and Q represents the service quality requirements of the relay system. We also set a maximum end-to-end experiment and a minimum availability probability to describe the signal-to-noise ratio threshold when specifying the circuit, and added maximum wind resistance, operating temperature range, and environmental dust protection level. In the task set T, for the sub-task of regional task coverage, the index of several thousand is expressed by the number of UAVs. The number of clusters and the communication model have a certain coupling relationship. The received signal under the model propagation in free space is represented by Formula (1) [19, 20].

$$P_r = P_t + G_t + G_r - 20\log_{10}(d) \\ -20\log_{10}(f) - 32.44 \tag{1}$$

In Formula (1), P_t indicates the drone's transmission power. G_t and G_r represent the gain of the transmitting and receiving antennas, respectively. Communication quality $P_r \geq RX_{sens} + SNR_{min}$ needs to be met. RX_{sens} represents the corresponding receiver sensitivity. SNR_{min} represents the minimum signal-to-noise ratio used. The above parameters can be used to calculate the expected maximum reliable communication distance, expressed as follows: d_{max} is rectangular and requires full coverage with no redundancy, then the minimum number of drones can be approximately estimated. See Formula (2) [21-23] for details.

$$N_{min} \approx \left\lceil \frac{L_x \cdot L_y}{\pi \cdot (d_{max}/2)^2 \cdot \eta} \right\rceil \tag{2}$$

In Formula (2), L_x and L_y is the range of the side length of the target region. η represents the overlap coefficient considering deployment efficiency. N_{min} is a quantitative relationship used to describe the basic information of cluster control and resource allocation.

At the next level, the core indicators are concentrated on three indicators: endurance, payload, and maximum cruising speed. Endurance is closely related to the duration of the mission, but a certain safety margin needs to be added, as shown in Formula (3) [24].

$$E_{total} = (P_{hover} + P_{avionics} + P_{com}) \cdot T_{mission} \cdot \eta_{sys}^{-1} \tag{3}$$

In Equation (3), the total available energy in the airborne energy pool is expressed as: E_{total} , the hovering energy consumption of drones is P_{hover} . $P_{avionics}$ refers to the power consumption of the entire system. P_{com} is the energy consumption relationship representing the communication payload. η_{sys} represents the conversion efficiency of the system's energy thruster, which ranges from 0.7 to 0.85. Therefore, the power consumption during hovering can be calculated, as shown in Formula (4).

$$P_{hover} = \frac{(m_{total} \cdot g)^{3/2}}{\sqrt{2\rho A} \cdot \eta_{rotor}} \tag{4}$$

In Formula (4), the total mass of the drone is expressed as m_{total} .We use g to represent the overall gravitational acceleration and ρ to represent the overall air density. A represents the total area swept by all drones during their patrols. η_{rotor} is used to represent the efficiency of the entire cruise system. We also define a total mass. m_{total} These masses are the sum of the masses of the entire system, including the frame, power, avionics, and communication loads. Therefore, the payload capacity can be expressed as Equation (5).

$$m_{payload} = m_{total} - (m_{frame} + m_{motor+ESC+prop} + m_{battery} + m_{avionics}) \geq m_{com} \tag{5}$$

In Formula (5), m_{com} represents the mass in a communication device. Formula (5) illustrates a coupling relationship. Increasing battery mass may result in minimal or even a decrease in battery life gain, because increasing the total mass E_{total} . At the same time, it will increase E_{total} , and will improve P_{hover} .Therefore, we need to make trade-offs to optimize our system.

In the above process, we represent the system as a comprehensive optimization problem with multiple objectives and constraints. We design the decision vector X as a global variable containing various parameters, including rotor diameter, motor KV value, battery energy density, and topology parameters. The optimization function is represented as F(X). It includes three main objectives: maximizing range, maximizing effective payload ratio, and minimizing cost. The constraints include strength constraints, dynamic constraints, thermal constraints, and electromagnetic constraints. We have established a quantitative analysis model, as shown in the figure. Specifically, it is illustrated in Equation (6).

$$P_{RX}^{noise-floor} = 10\log_{10}(10^{P_{thermal}/10} + 10^{(P_{emit} - I_{isolation})/10}) \tag{6}$$

The decision vector is explicitly redefined as $X = [D_r, K_v, E_{batt}, T_{topo}]$ representing rotor diameter, motor KV value, battery energy density, and topology parameters, respectively, to ensure full reprehensibility. $P_{RX}^{noise-floor}$ represents the noise floor at the receiver input. The transmit level of the interference source is expressed as $P_{thermal} = 10\log_{10}(kTB)$ Isolation that can be achieved through layout optimization, shielding filtering, and other methods can be expressed as P_{emit} The design goal of this process is to ensure a sensitive reception process by increasing. The specific quantitative analysis model is shown in Figure 1.

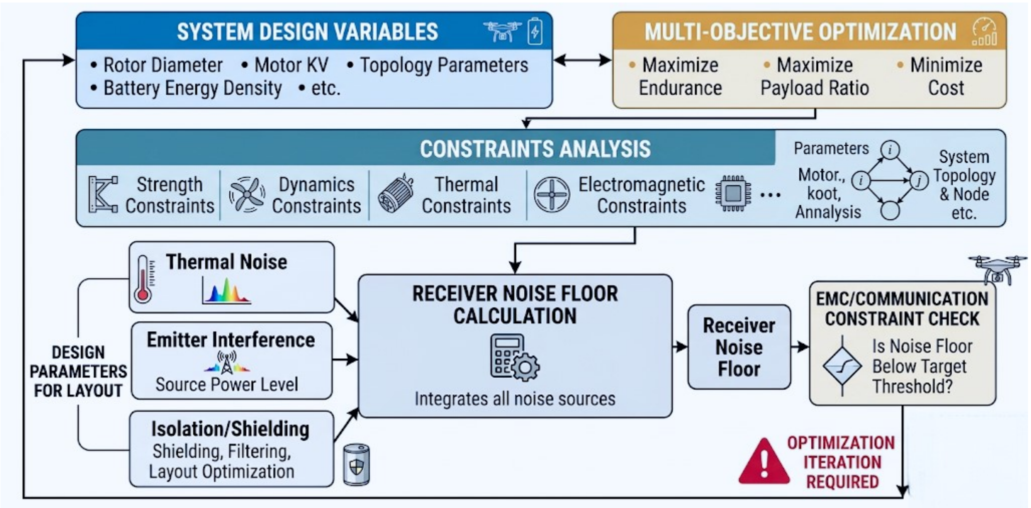

Figure 1. Quantitative Analysis Model

3.2 Comprehensive Modeling of Uncertain Cluster Systems

To construct a reliable distributed algorithm, we aim to build a comprehensive mathematical model of the various characteristics of UAV swarms in low-altitude environments. In this model, we consider the i-th multi-wing UAV and decompose its motion into outer-loop position control and inner-loop attitude control. For cooperatively controlled UAV swarms, we focus more on the dynamics of the outer loop, especially during low-speed flight. The dynamics can be described using integrators as shown in Equations (7) and (8).

$$\dot{\mathbf{p}}_i(t) = \mathbf{v}_i(t) \tag{7}$$

$$\dot{\mathbf{v}}_i(t) = \mathbf{u}_i(t) + \mathbf{d}_i(t) \tag{8}$$

In Equations (7) and (8), the position of the UAV in inertial coordinates during this process is represented by $\mathbf{p}_i(t) = [x_i(t), y_i(t), z_i(t)]^T \in R^3$. $\mathbf{v}_i(t) \in R^3$ represents a velocity vector during the drone's movement. $\mathbf{d}_i(t) \in R^3$ is its control input vector. We treat it as a command to change acceleration.

This command is ultimately implemented by the attitude controller, thus being translated into a motor speed command. We use an interactive graph approach to represent a changing directed acyclic graph.

Nodes represent all corresponding drone nodes in the cluster, and edge sets represent communication circuits at different times. If, at a certain time, there is an available communication link between drone i and drone j, then the adjacency matrix corresponding to the directed graph will change.

Furthermore, in low-altitude environments, due to obstacles and other factors, the connection of communication links is probabilistic; therefore, we must transform the edge set modeling into a stochastic process, as shown in Equation (9).

$$\begin{aligned} p_{ij}(t) &= P\left(a_{ij}(t) = 1\right) \\ &= f\left(\| \mathbf{p}_i(t) - \mathbf{p}_j(t) \|, \phi_{ij}(t), \Gamma_{ij}(t)\right) \end{aligned} \tag{9}$$

In Formula (9). $\| \mathbf{p}_i - \mathbf{p}_j \|$ is used to represent a non-increasing function. We can estimate it using geometric relations and empirical model-based methods. $\phi_{ij}(t)$ is parameter.

3.3 Joint Scheduling of Communication Energy and Resources Across Three Terminals

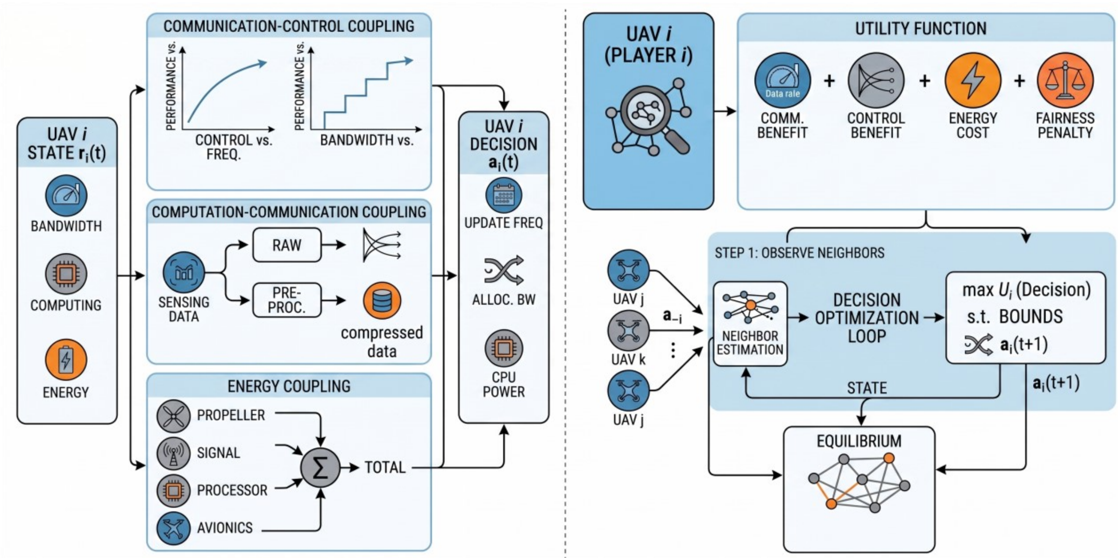

Figure 2. Joint Scheduling Process

Figure 2 illustrates the cross-resource communication joint scheduling process. The drones consider their initial state, including bandwidth, computing power, energy consumption, and the coupling relationships between various resources, thus making a locally optimal decision. On the right side of the figure, we represent each drone as a rational player. Players observe their neighbors' states based on a predefined utility function to optimize their decisions.

We perform unified modeling and analysis of resources across three dimensions—communication, computing, and energy—at the cluster level.

We define the resources of UAV i as triples within a time interval t. $\mathbf{r}_i(t) = [B_i(t), C_i(t), E_i(t)]^T$ This represents the currently available bandwidth resources, computing resources, and remaining energy. We describe the decision-making action variables as $\mathbf{a}_i(t) = [f_i^{ctrl}(t), b_i(t), c_i^{proc}(t)]^T$ Specifically, it can represent changes in control frequency, allocated bandwidth, and CPU computing power applicable to local processing capabilities. We perform unified performance modeling and analysis by coupling modules, specifically by coupling communication and control, and computation and communication. Communication and control coupling creates a dependency between system performance and control frequency.

The system's stability, accuracy, convergence speed, and communication bandwidth (B) are closely related. High-frequency control requires $B_i^{used}(t) \propto f_i^{ctrl}(t) \cdot S_{msg}$ significantly more bandwidth to transmit status commands. S_{msg} represents the size of the message during this process.

The computation-communication coupling involves a trade-off analysis between local computation and direct transmission of sensor data. Local preprocessing can significantly reduce the amount of compressed data and save bandwidth. Conversely, direct transmission can also conserve local computing power. c_i^{proc} However, this could lead to a bottleneck in overall bandwidth resources. Energy coupling is the sum of the total power consumption of a node, including the total energy consumed during communication and computation.

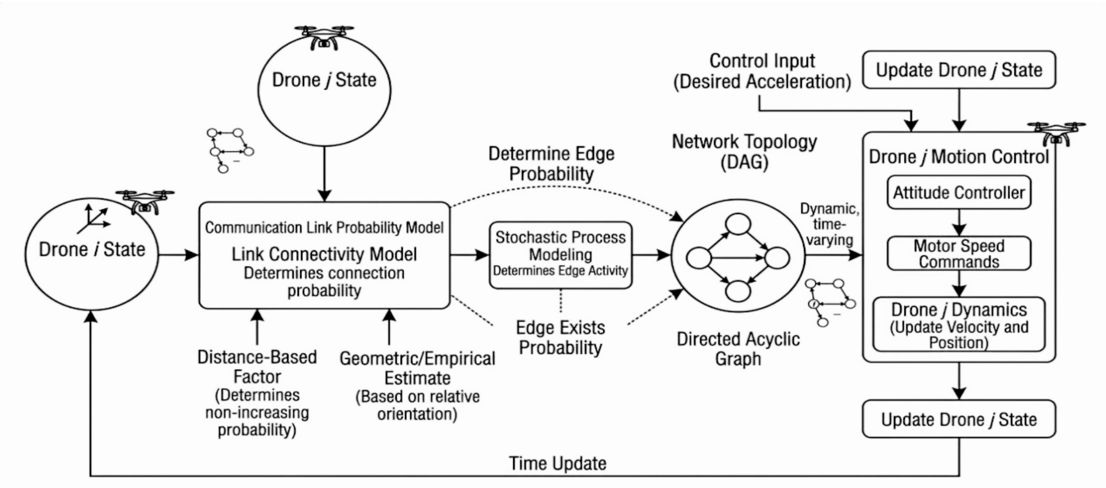

Figure 3. Distributed Resource Allocation Model

As shown in Figure 3, we constructed a distributed resource allocation model based on game theory. We represent the drones in the cluster as decision-makers, characterized by rationality and self-interest. Each decision-maker's core objective is to maximize their own effect by adjusting their strategy within the constraints of limited resources. The effect of player i is not only related to their own strategy but also influenced by the strategies of other players in the player interaction network. In this process, we represent the utility function as a comprehensive cost-benefit evaluation system, as shown in Equation (10).

$$U_i(\mathbf{a}_i, \mathbf{a}_{-i}) = \omega_1 R_i^{com} + \omega_2 Q_i^{ctrl} - \omega_3 P_i^{total} - \omega_4 F_i \quad (10)$$

In Equation (10), ω_1 'to ω_4 ' represents the positive weight parameters of the model, representing the coefficients of different dimensional objectives. Specifically, these include positive rewards and negative penalties. The communication reward is shown by analyzing the reachability of data using the Shannon formula, which is closely related to its bandwidth and power. The control reward is used to analyze indicators related to consistency errors.

The negative cost penalty includes the total power consumption used in this process, i.e., energy cost. In addition, there is a fairness penalty; for example, individual nodes maliciously occupying public resources will incur a certain degree of penalty to encourage fair allocation among nodes. In terms of solution, we perform local problem optimization for each drone, as shown in Equations (11) and (12).

$$\max_{\mathbf{a}_i \in \mathrm{A}_i} U_i(\mathbf{a}_i, \mathrm{E}[\mathbf{a}_{-i}]) \quad (11)$$

$$\text{s.t.} \quad b_i \le B_i^{avail}, \quad c_i^{proc} \le C_i^{avail}, \quad E_i \ge E_{min} \quad (12)$$

As shown in Formulas (11) and (12), the parameters A_i represent the set of feasible options for this strategy. The solution to the distributed game problem ultimately points to a Nash equilibrium, or NE node. At an NE node, no single drone can unilaterally change its strategy to optimize the overall effect. In each iteration, the drone updates its own strategy based on the observed states of its neighbors, eventually leading to convergence of all files in the network, reaching an equilibrium state, and ultimately optimizing overall resources and achieving the globally optimal solution.

Table 1. Simulation Experiment Configuration Parameter Table

Parameter categories	Parameter name	Parameter value/description
Scene settings	Area size	200 m × 200 m
	Obstacle	Randomly distributed, at a height of 20-50 m
	Communication model	Logarithmic shadow path loss + probabilistic Loss
Cluster configuration	Number of drones	4 aircraft, 8 aircraft (compare scalability)
	Initial formation	Square formation, 20 m apart
	Communication radius	50 m
Algorithm configuration	Comparison Algorithm	LF, Consensus (Ideal)
	Proposed Algorithm	Robust Consensus + Event-triggered + Coverage
Disturbance settings	Wind disturbance model	Dryden turbulence model, maximum wind speed 8 m/s
	Communication constraints	Latency: 0-100ms random; Packet loss rate: 0-20%

4. Simulation Platform Construction and Result Comparison

4.1 Experimental Design

Table 2. Core Configuration Table of Unmanned Aerial Vehicle Swarm Prototype

System Module	Components/Parameters	Specifications/Model/Values
Flight platform	rack type	Custom quadcopter, made of carbon fiber, with a wheelbase of 550 mm
	Powertrain	T-Motor F60 Pro motor + 45A ESC + 1245 propellers
	Energy System	6 S 10000 mAh lithium polymer battery
	Theoretical range	No load ≥ 40 minutes, full load (communication load) ≥ 25 minutes
Navigation and Control	Flight control	Pixhawk 6C (running PX4 Autopilot)
	position	Integrated navigation: RTK GPS (centimeter-level accuracy) + Intel RealSense T265 visual odometry
	Onboard computer	NVIDIA Jetson Xavier NX
Communication and networking	Self-organizing network radio	Customized dual-band (2.4 G/5.8 G) mesh module, maximum power 1 W.
	protocol	TDMA protocol based on IEEE 802.11 s extension
	Data Link	Data radio (used for ground monitoring and security commands)
Mission payload	Cooperative communication payload	Software radio module (USRP B210) can simulate 4 G/5 G micro base stations.
	Perception	Intel RealSense D435i Depth Camera (Obstacle Avoidance and Local Mapping)

To fully demonstrate the effectiveness of our methodology, we conducted not only virtual system simulations but also systematic investigations using physical prototypes. We built a co-simulation environment using MATLAB and iOS. A digital twin model was created for testing the swarm algorithm, incorporating PX4 flight control and iOS. A hardware-in-the-loop simulation system was also used, integrating the physical flight control hardware into the overall simulation loop to verify the algorithm's actual performance. We used four UAVs as swarm prototypes, simulating typical air-to-ground cooperative tasks. Our verification tasks included dynamic formation keeping, communication relay, and connectivity coverage. Our simulation design utilized a 200x200 simulated area, specifically a canyon terrain, with randomly distributed obstacles. The UAV swarm needed to operate within this area.

Coordination during this process required maintaining dynamic ad hoc network communication. To evaluate the model, we also referenced several classic methods. First, we used the pilot-follower method and the distributed consensus algorithm as two baseline models. In terms of metrics, we considered root mean square error, system energy consumption, network connectivity, and communication load, among other capabilities. Specific parameters for our experiments are shown in Table 1. Furthermore, we presented a description of the UAV prototype used for field flight verification, showcasing its core design and detailed configuration, as shown in Table 2. We also presented the hyperparameters used in the model experiments and evaluation. Sensitivity analysis of the hyperparameters was performed during the experiments, and the specific hyperparameter list is shown in Table 3.

Table 3. Hyperparameter Setting Table for Core Algorithm

Algorithm Module	Hyperparameters	Symbol	Setting value	Setting basis
Robust consistency control	Position gain	kp	0.8	Balancing convergence speed and overshoot
	Speed gain	kd	1.2	Provide damping and stabilization system
	Adaptive gain	η	0.05	Ensure the speed and stationarity of disturbance estimation
Event triggering mechanism	relative threshold coefficient	α	0.6	Balancing communication savings and control accuracy
	absolute threshold	β	0.1 m	To prevent infinite non-triggering
Coverage-connectivity control	Coverage gain	kc	0.5	Controlling the velocity of motion toward the Voronoi center of mass
	Connected potential field weight	κ	10	Ensure sufficient repulsive force is generated at the edge of the communication radius.
	Communication radius warning value	Ra	40m (less than Rc)	Prematurely triggering connectivity maintenance behavior

4.2 Experimental Results

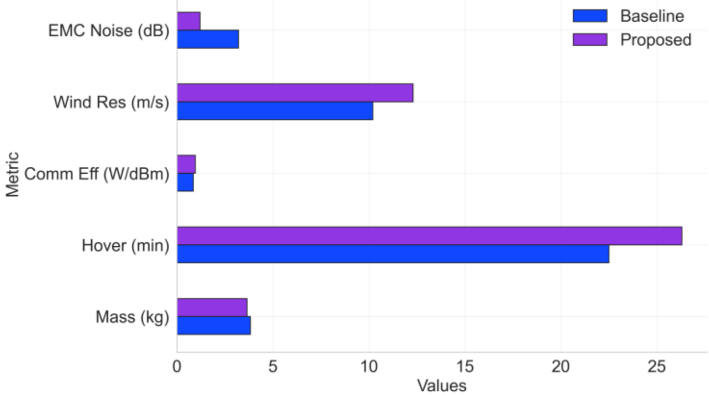

Figure 4. Task-Throughput-Lifetime Improvement in Resource Co-Optimization

As shown in Figure 4, we present the model's performance under three metrics: task completion rate, throughput, and lifetime. The results show that, transitioning from a no-scheduling scenario to a fully joint optimization scenario, the task completion rate increased from 80% to 95%, the throughput increased from 22 Mbps to 33 Mbps, and the lifetime extended from 31 minutes to 58 minutes.

Our performance evaluation primarily involves conducting extensive simulation tests to statistically analyze various metrics. Furthermore, during actual flight, we acquire status data via ground stations and use onboard testing software to perform end-to-end throughput, latency, and packet loss tests to evaluate overall performance. Table 4 shows a comparison of formation accuracy under different algorithmic conditions. We set up three scenarios: wind disturbance, communication experiment, and packet loss.

The proposed algorithm maintains the highest overall formation accuracy and exhibits significant advantages in robustness and consistency compared to other algorithms. The results show that the centralized and hierarchical models perform reasonably well under no disturbance conditions, but their performance drops sharply under disturbance conditions. Under combined disturbance conditions, the error reaches 1.23 meters, indicating a high dependence on low-altitude links and global information. We also considered the analysis of classic consensus protocols, a representative algorithm of distributed control. Under ideal communication conditions, it maintains a high level of accuracy, reaching 0.05 meters. However, its performance significantly degrades under communication latency and packet loss, indicating that classic consensus protocols have high requirements for overall communication quality.

Table 4. Comparison of Formation Keeping Accuracy under Different Control Algorithms

Algorithm/Condition	No wind and no disturbance	Maximum gust 8 m/s	Latency 0-100ms	Packet loss rate 0-20%	Combined disturbances (wind + latency + packet loss)
Navigation-Following Method (LF)	0.12 m	0.85 m	0.51 m	0.47 m	1.23 m
Classical Consistency (Ideal)	0.05 m	0.61 m	0.76 m	0.69 m	1.12 m
Robust Consistency (This paper)	0.08 m	0.32 m	0.28 m	0.25 m	0.41 m
Robust consistency + event triggering	0.10 m	0.35 m	0.31 m	0.29 m	0.45 m
Robust consistency + event triggering + coverage control	0.15 m	0.40 m	0.36 m	0.33 m	0.52 m

In Table 5, we conducted real-world tests at low altitudes from a collaborative design perspective, considering the limited bandwidth of the autonomous network and the energy constraints of the UAV. Our experimental analysis shows that, based on a theoretical foundation, we set the ideal communication cycle to 1 millimeter. Under this condition, communication costs are high; updating once at 1000 Hz consumes 3200 kbps of bandwidth. The highest accuracy is achieved under this condition, while with a communication cycle of 50 milliseconds, the bandwidth and energy consumption decrease significantly, but the loss is substantial, increasing by 15.2%. Under the fixed threshold triggering condition, compared to periodic communication, it is more intelligent, with an accuracy loss of only 8.7% and a trigger interval of only 0.182 milliseconds, showing a more significant advantage for the relative threshold triggering mechanism presented in this paper. The core advantage of this paper lies in the correlation between the triggering conditions and the current cooperative error. This means that if the system is stable, i.e., the error state is small, the communication mechanism itself, even with a small bias, will not trigger relatively unnecessary communication. However, when the error increases, it will communicate more frequently to quickly stabilize the overall system. Therefore, among all models, our indicators achieve a better balance, with the lowest communication frequency of only 4.26 Hz and the smallest bandwidth usage of 13.63 kb. This also results in greater energy savings compared to other models.

Table 5. Communication Load Reduction Effect under Event-Triggered Communication Mechanism

Scene/Algorithm	Average trigger interval (s)	Average packet sending frequency per machine (Hz)	Total bandwidth usage (Kbps)	Control accuracy loss (RMSE increased)	Energy saving (Communication Module)
Ideal communication (period 1ms)	0.001	1000	3200	Baseline 0.00%	0.0%
Periodic communication (period 50ms)	0.050	20	64	+15.2%	12.1%
Fixed threshold event triggering	0.182	5.5	17.6	+8.7%	21.3%
Relative threshold event triggering (this article)	0.235	4.26	13.63	+5.3%	26.8%
Adaptive threshold event triggering	0.251	3.98	12.74	+4.1%	28.5%

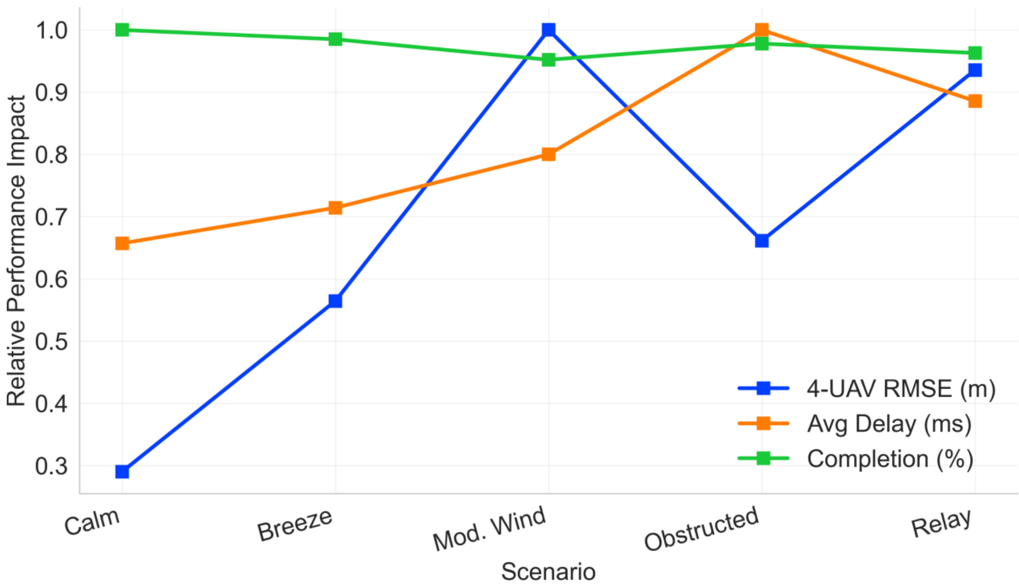

Figure 5. Effectiveness Verification of Uav Swarm Collaborative Control and Electromechanical Design

As shown in Figure 5, we use a line graph to illustrate the performance differences between our proposed method and the two baseline models under various perturbation scenarios, including a maximum gust of 8 m/s, a latency of 0–100 ms, and a packet loss rate of 0–20%. The results demonstrate the mean squared error (RMSE) and task completion rate. The proposed method shows a significant advantage in formation accuracy (RMSE) compared to traditional methods under strong disturbance conditions, and maintains a low error of only 0.52 cm even under perturbation conditions. The task completion rate consistently remains above 0.9, indicating strong robustness of our method to scenarios such as packet loss due to wind disturbance. The addition of coverage control slightly increases the RMSE to 0.52 m, but results in higher regional coverage and network connectivity.

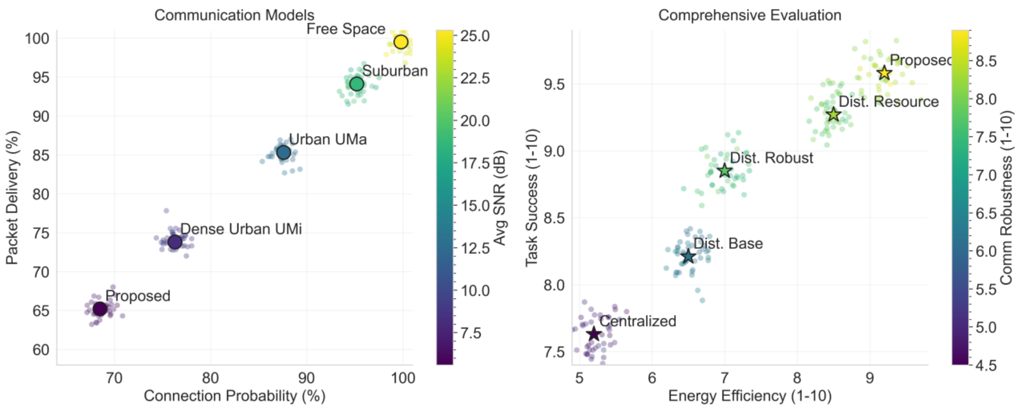

Figure 6. Trade-off between Communication Load and Accuracy Loss in Event-Triggered Communication Mechanisms

Figure 6 illustrates the overall impact of the time-triggered mechanism on communication complexity and control accuracy. We present this using a line graph, showing multiple metrics and results under different event-triggered scenarios. Our method of using a relative threshold trigger extends the average trigger interval by 0.235 seconds. Low packet transmission frequency: Increased to 4.26 Hz, bandwidth value used: 13.63 KPS. Ideal communication: Compared to this scenario, our model has significant advantages, with only a 5.3% control error loss and a 26.8% energy saving in the communication module. This demonstrates that our method, using a relative threshold, effectively controls accuracy loss by dynamically adjusting the cohesion consistency error as the trigger condition.

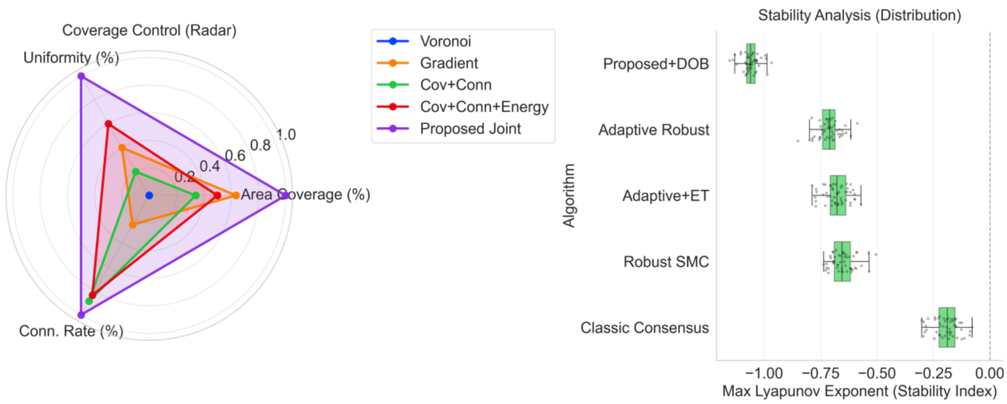

Figure 7. Comparison of Radar Charts for Coverage and Connectivity Control

Figure 7 shows a comprehensive comparison of coverage and connectivity. We also compared five control algorithms, and the results show that our proposed method achieves the best performance across all three metrics. The uniformity metric approaches 100%, and the area coverage exceeds 95%. This demonstrates that our method has significant advantages over traditional methods.

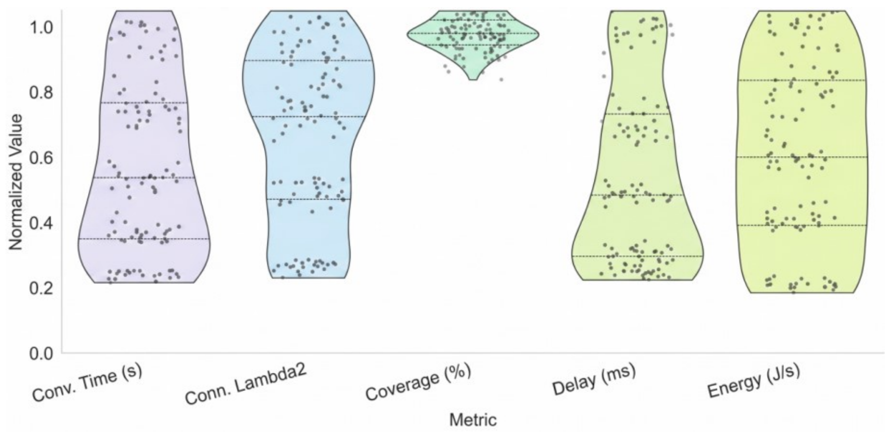

Figure 8. Distribution of Lyapunov Exponent for Algorithm Stability

Figure 8 shows the exponential distribution of algorithm stability. We compared five algorithms using box plots with Lyapunov exponents. These exponents are a new type of stability metric, with more negative values indicating greater stability. Using box plots to illustrate the stability distribution, the results show that our proposed method has an exponent close to -1.0, and the box plot distribution is very compact, indicating that our model has the best stability.

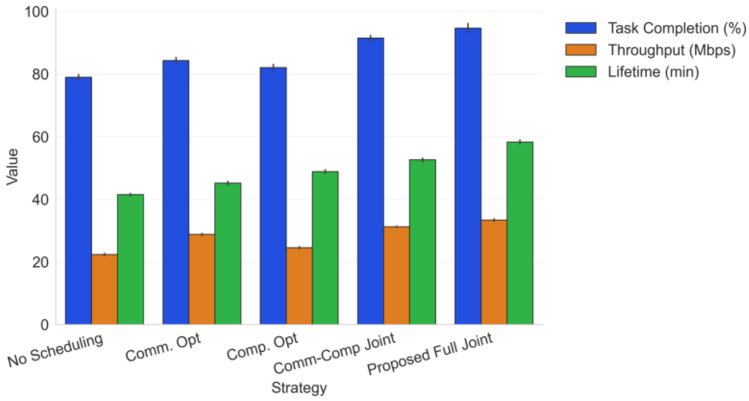

Figure 9. Performance Trade-Offs in Energy-Delay-Coverage Distribution

As shown in Figure 9, we present the overall performance of multiple metrics. We use a distribution plot to illustrate the normalized metrics and analyze multiple dimensions such as convergence time, connectivity, coverage, and energy consumption. The results show that the proposed algorithm leans towards the optimal range in multiple dimensions and does not exhibit poor performance in terms of experimental energy consumption, indicating that the model can achieve low latency, stable communication, and high coverage.

5. Conclusions

This paper systematically studies and empirically evaluates the collaborative optimization of UAV swarms in complex low-altitude scenarios. The core innovation lies in constructing a multidisciplinary collaborative design framework for electromechanical systems. This framework aggregates multiple top-level task indicators and transforms them into parameters for UAV design. The NSGA algorithm is used to solve this problem, obtaining a theoretically optimal solution that meets the requirements of multiple tasks. Furthermore, a swarm integration model with dynamic communication constraints is modeled, and a distributed control algorithm is constructed to achieve robust adaptation. Based on this, a decision-making framework integrating fusion, coverage, and connectivity control is built. Combining Voronoi segmentation with connectivity maximizes UAV coverage while avoiding communication interruptions due to excessive distance. The current study firmly establishes the feasibility and significant performance gains of the integrated framework through high-fidelity hardware-in-the-loop simulations. However, it is acknowledged that broader real-world validation, particularly in dynamic urban canyons and extreme weather conditions, remains an open challenge. The present results serve as a crucial benchmark and proof-of-concept, demonstrating that the proposed joint optimization offers a scalable and energy-efficient foundation. Future work will prioritize field tests under diverse operational environments to bridge the simulation-to-reality gap.

Funding

This study was supported by University-level Teaching Reform Project “The Integration of Production-Oriented Teaching and OBE: Teaching Reform Practice of Analog Electronic Technology in Vocational Undergraduate Courses” (No: JG250010).

References

[1] Gräfe, A., Eickhoff, J., Zimmerling, M., & Trimpe, S. (2025). DMPC-Swarm: distributed model predictive control on nano UAV swarms. Autonomous Robots, 49(4), 53. https://doi.org/10.1007/s10514-025-10211-w

[2] Li, J. H., Sun, G., Wu, Q. Q., Liang, S., Wang, J. C., Niyato, D., & Kim, D. I. (2026). Aerial secure collaborative communications under eavesdropper collusion in low-altitude economy: a generative swarm intelligent approach. IEEE Transactions on Mobile Computing, 25(4), 5758–5774. https://doi.org/10.1109/tmc.2025.3633953

[3] Yang, Z. Z., Cui, Y. H., & Li, Y. M. (2026). Transformer-based cooperative UAV encirclement policies under uncertainty in low-altitude wireless networks. IEEE Transactions on

Cognitive Communications and Networking, 12, 3525–3537. https://doi.org/10.1109/tccn.2025.3632389

[4] Wang, F., Yang, H. T., Zhang, S. Y., Shi, J., Li, Z., & Quek, T. Q. S. (2025). Mobility-aware multicast orchestration for low-altitude UAVs with integrated terrestrial and non-terrestrial networks. IEEE Transactions on Communications, 73(11), 12854–12868. https://doi.org/10.1109/tcomm.2025.3591176

[5] Geng, X. S., Tang, K. H., Guo, Y., Zhang, L., Wu, W. Q., & Ma, T. F. (2025). A distributed UAV swarm countermeasure method based on GNSS spoofing. IEEE Internet of Things Journal, 12(16), 33455–33467. https://doi.org/10.1109/jiot.2025.3575080

[6] Jiang, S., Chi, P., Yang, L. N., Liu, Y. H., Zhao, J., & Wang, Y. X. (2026). Self-organizing distributed target fencing of UAV swarm for an uncooperative target. Aerospace Science and Technology, 176, 112130. https://doi.org/10.1016/j.ast.2026.112130

[7] Suo, W. B., Wang, M. Y., Zhang, D., Qu, Z. J., & Yu, L. (2022). Formation control technology of fixed-wing UAV swarm based on distributed Ad hoc network. Applied Sciences, 12(2), 535. https://doi.org/10.3390/app12020535

[8] Zhao, J., Sun, J. M., Cai, Z. H., Wang, Y. X., & Wu, K. (2022). Distributed coordinated control scheme of UAV swarm based on heterogeneous roles. Chinese Journal of Aeronautics, 35(1), 81–97. https://doi.org/10.1016/j.cja.2021.01.014

[9] Lin, M. T., Li, B., Zhou, B., & Cecati, C. (2025). Distributed stochastic model predictive control for heterogeneous UAV swarm. IEEE Transactions on Industrial Electronics, 72(7), 7384–7394. https://doi.org/10.1109/tie.2024.3508055

[10] Delansnay, G., Ocampo-Martinez, C., Dewasme, L., & Vande Wouwer, A. (2026). Partitioning and distributed predictive control of UAV swarms. Robotics and Autonomous Systems, 202, 105473. https://doi.org/10.1016/j.robot.2026.105473

[11] Bao, Y. Y., Cheng, X. C., Nie, L. M., & Tao, J. Y. (2026). Enabling privacy-preserving and drop-out resilient federated LLM fine-tuning for the low-altitude UAV swarm networks. IEEE Transactions on Cognitive Communications and Networking, 12, 2919–2936. https://doi.org/10.1109/tccn.2025.3620369

[12] Feng, L., Zheng, H., Zhao, Y. K., Zhou, F. Q., Li, W. J., & He, F. (2026). Autonomous flight control for UAV swarm using evolutionary multi-agent multi-objective reinforcement learning. IEEE Transactions on Cognitive Communications and Networking, 12, 4673–4686. https://doi.org/10.1109/tccn.2025.3643996

[13] Gao, N., Liang, L., Cai, D. H., Li, X., & Jin, S. (2022). Coverage control for UAV swarm communication networks: a distributed learning approach. IEEE Internet of Things Journal, 9(20), 19854–19867. https://doi.org/10.1109/jiot.2022.3170123

[14] Zhu, B. T., & Deng, Y. M. (2023). Distributed UAV swarm control framework with limited interaction for obstacle avoidance. Aircraft Engineering and Aerospace Technology, 95(5), 697–705. https://doi.org/10.1108/aeat-04-2022-0099

[15] Dong, C., Zhang, Y. F., Jia, Z. Y., Liao, Y. Y., Zhang, L., & Wu, Q. H. (2025). Three-dimension collision-free trajectory planning of UAVs based on ADS-B information in low-altitude urban airspace. Chinese Journal of Aeronautics, 38(2), 101152. https://doi.org/10.1016/j.cja.2024.08.001

[16] Liu, R. X., Le, X. L., Gu, S., Lv, S. L., Mao, P. D., & Quan, Q. (2026). Distributed network control of multi-UAV systems for cooperative heavy-load transport using a virtual-passivity framework. IEEE Transactions on Network Science and Engineering, 13, 5905–5923. https://doi.org/10.1109/tnse.2026.3654107

[17] Ding, Y. H., Yang, Z. H., Pham, Q. V., Hu, Y., Zhang, Z. Y., & Shikh-Bahaei, M. (2024). Distributed machine learning for UAV swarms: computing, sensing, and semantics. IEEE Internet of Things Journal, 11(5), 7447–7473. https://doi.org/10.1109/jiot.2023.3341307

[18] Alam, M. M., & Moh, S. (2024). Joint optimization of trajectory control, task offloading, and resource allocation in air-ground integrated networks. IEEE Internet of Things Journal, 11(13), 24273–24288. https://doi.org/10.1109/jiot.2024.3390168

[19] Jin, Y., Deng, Z. L., Zhang, H., Ding, Z. K., Tang, X. Y., & Wang, Z. L. (2026). A review of UAV positioning in LAIN: toward a 5G-Core "Space-Air-Ground" integrated and cooperative architecture. Engineering Information Technology & Electronic Engineering, 27(1), 1–16. https://doi.org/10.1631/eng.Itee.2025.0127

[20] Li, J. Q., Li, J. J., Zhang, J., & Meng, W. Y. (2025). A comprehensive review of path-planning algorithms for multi-UAV swarms. Drones, 10(1), 11. https://doi.org/10.3390/drones10010011

[21] Dou, W. Y., Yang, P., Zhang, Z. W., & Wang, Z. H. (2025). Cooperative multi-uav search for prioritized targets under constrained communications. Drones, 9(12), 855. https://doi.org/10.3390/drones9120855

[22] Niu, B. J., Fan, H. J., Liu, L., & Wang, B. (2025). Distributed output-feedback containment control for UAV swarm with input saturation under distributed DoS attacks. Asian Journal of Control, 27(6), 3070–3084. https://doi.org/10.1002/asjc.3654

[23] He, H. X., Huo, M. Z., Duan, H. B., Deng, Y. M., & Wei, C. (2025). Distributed cooperative control of human-UAV swarm based on state observation. IEEE Transactions on Systems, Man, and Cybernetics: Systems, 55(10), 7335–7345. https://doi.org/10.1109/tsmc.2025.3584209

[24] Li, Y. B., Zhang, Z. T., Huang, Y. J., Sun, Q., & Dong, Q. H. (2025). DFASCN: A distributed flocking approach for UAV swarm collective navigation. Future Generation Computer Systems, 171, 107852. https://doi.org/10.1016/j.future.2025.107852